Wiley Analytical Science

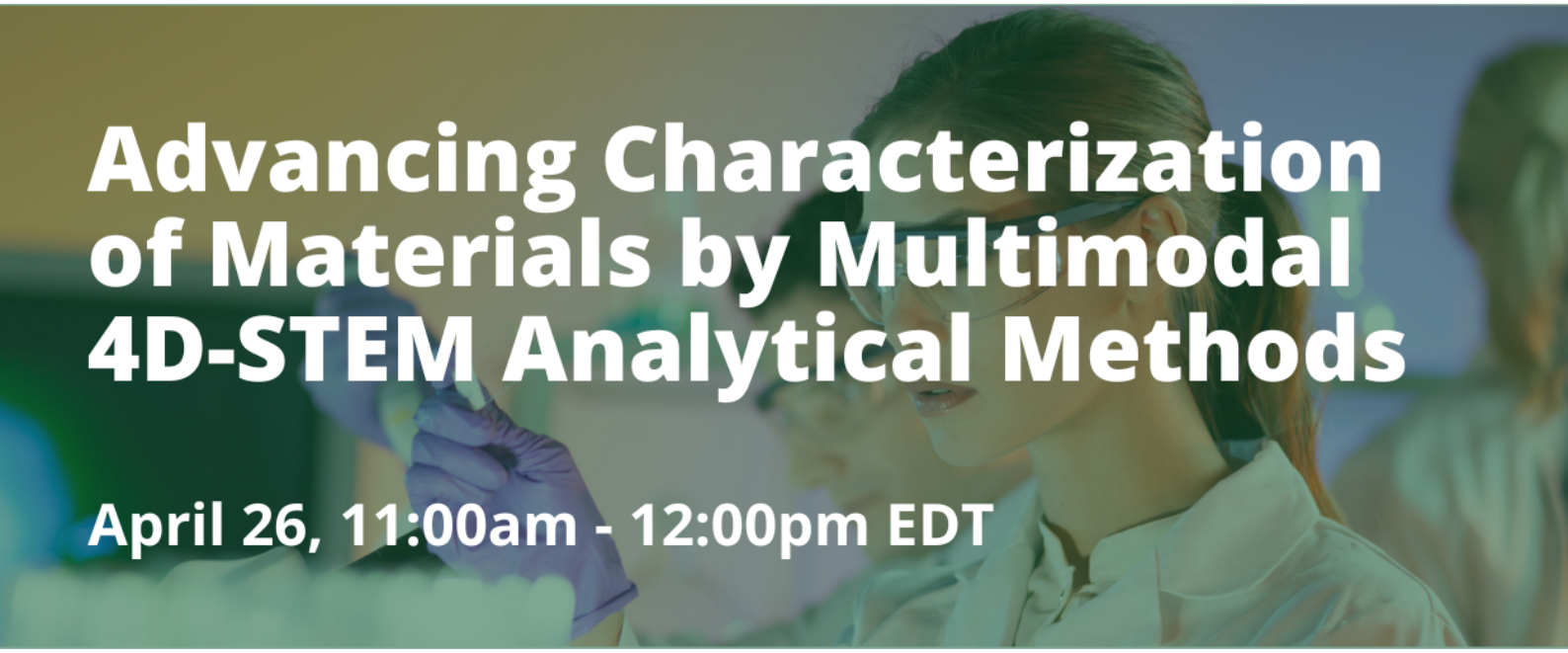

Advancing Characterization of Materials by Multimodal 4D-STEM Analytical Methods

April 26, 11:00am - 12:00pm EDT

Development and production of new materials and semiconductor devices require morphological, structural, and chemical characterization at the nanoscale level to understand their chemico-physical properties and optimize their production process. Besides traditional electron microscopy imaging and compositional analysis techniques, 4D-STEM methods provide additional structural information about the local internal organization of atoms and molecules at each position of an acquired STEM map.

Watch this session during the WAS Virtual Conference:

Dr. Daniel Nemecek

Dr. Tingting Yang

Register Now

This talk is sponsored by TESCAN
PERFORMANCE IN NANOSPACE

ADVANCED OPTICAL MATERIALS
www.advopticalmat.de

Halide Perovskite Excitonic Diffraction Grating

Mariia P. Mamaeva, Maksim S. Lozhkin, Anna V. Shurukhina, Boris V. Stroganov, Alexei V. Emeline, and Yury V. Kapitonov*

Resonant diffractive optical elements can be used to create the desired spatial and angular distribution of scattered light in a narrow wavelength range. Exciton resonance could help to make such elements active. Here an exciton diffraction grating made from fully inorganic $CsPbBr_3$ halide perovskite is demonstrated. Spatial modulation of excitonic properties of the single crystal is achieved using local defect formation by 30 keV Ga^+ focused ion irradiation with low irradiation dose 10^{14} cm^{-2}. Such a low dose prevents the appearance of non-resonant diffraction since no sample milling occurs. The observed diffraction reflex has a maximum efficiency of 2.3×10^{-3} at the free exciton resonance and 1.7 meV spectral width. The temperature, angular, and spectral properties of resonant diffraction are studied. The possibility of creating exciton diffraction gratings based on halide perovskites is one more confirmation of their applicability as a new material for information photonics.

1. Introduction

Light is considered a carrier of information in the information photonics. To process information in a purely optical way, active elements are needed. The material excitations in them must effectively interact with light, and be nonlinear and resonant. Excitons, which are a bound state of an electron and a hole, as well as various exciton complexes, are suitable for this role in direct-gap semiconductors.

The coherent response from an ensemble of excitons could be demonstrated in the reflection of light from a flat or semi-infinite ensemble—an excitonic mirror.[1,2] Excitons are excited when a plane monochromatic wave with the energy E equal to the exciton resonance energy E_{exc} is incident on such an ensemble. Each exciton re-emits light with a phase determined by the phase of the incident wave. The interdependency of the emission phases of individual excitons makes it possible to form coherent transmitted and reflected plane waves. Such a response will be resonant since it will vanish as the light energy is detuned from the exciton resonance. The spectral width of the reflectivity will be determined by the exciton ensemble radiative width (which is proportional to the exciton oscillator strength), homogeneous, and inhomogeneous broadenings. The study of reflection spectra is somewhat complicated due to the presence of non-resonant reflection from the sample surface. The Brewster geometry could be used to suppress this non-resonant background.[3]

The spatial modulation of exciton optical properties could be used to control the spatial-angular properties of the coherent response of the ensemble. The simplest example of such modulation is the excitonic diffraction grating.[4–7] Such modulation leads to the formation of diffraction reflexes and could be used to control the light propagation direction. These reflexes are also resonant, and non-resonant background is not observed in their spectra since only excitonic properties are modulated. Another example of control of the light propagation direction is the reflection from an ensemble with the gradient of the exciton resonance energy.[8] All these examples could be grouped under the term excitonic diffractive optical elements (DOEs). Finally, the random modulation will lead to the resonant Rayleigh scattering.

To create excitonic DOEs, local modulation of exciton properties is required on a scale close to the wavelength of light. The readily-accessible approach is the modulation of the inhomogeneous broadening since it depends on the crystal imperfections and could be modulated by the local introduction of defects. We have proposed two methods for the local defect formation for "classic" GaAs-based structures: epitaxial growth on a substrate preliminary irradiated by focused ion beams (FIB)[4] and ion irradiation of samples after epitaxial growth.[6] In both cases, periodic modulation of the inhomogeneous broadening of exciton resonances in the quantum well made it possible to create an exciton diffraction grating with the optical properties described above.

Halide perovskites recently have attracted attention as semiconductor materials for photovoltaics,[9] light-emitting diodes,[10] and microlasers.[11–15] Wannier–Mott excitons with binding energies of tens of meV were observed in three-dimensional halide perovskites.[16–19] Restricting the movement of excitons in low-dimensional perovskite-like compounds makes it possible to obtain binding energies of hundreds of meV.[20,21] Halide perovskites are considered promising nonlinear optical materials.[22] Photon echo has been observed in halide perovskites.[23–25] All of the above, as well as the simple liquid-phase synthesis and the ability to adjust the band gap in the entire visible range by anion substitution, make the family of halide perovskites proper for information photonics applications.

M. P. Mamaeva, M. S. Lozhkin, A. V. Shurukhina, B. V. Stroganov, A. V. Emeline, Y. V. Kapitonov
Saint Petersburg State University
Ulyanovskaya d.1, St. Petersburg 198504, Russia
E-mail: m.mamaeva@spbu.ru

The ORCID identification number(s) for the author(s) of this article can be found under https://doi.org/10.1002/adom.202202152.

DOI: 10.1002/adom.202202152

To create an excitonic DOE based on halide perovskites, it is also possible to use FIB. The milling of halide perovskites by ion beams is well-studied.[26,27] However, to create resonant DOEs, it is necessary to use doses well below the milling dose 10^{16} cm^{-1}. Irradiation of $CsPbBr_3$ and $MAPbI_3$ ($MA^+ = CH_3NH_3^+$) halide perovskites with such doses of 30 keV Ga^+ or He^+ ions leads to the formation of defect serving as radiative recombination centers.[28–30] The irradiation with meV ion beams leads to the increase in the emission of $MAPbBr_3$.[31] Such behavior could be explained by the well-known defect tolerance of these materials[32] which gives hope for the possibility of careful modulation of excitonic properties by FIB.

In this work, we demonstrate the simplest excitonic DOE, excitonic diffraction grating, made by irradiation of $CsPbBr_3$ halide perovskite with the 30 keV Ga^+ FIB. The irradiation doses are well below the doses required for sample milling. Due to this, a local periodic modulation of exclusively excitonic properties was made and a directed spectrally narrow diffraction reflex emerges.

2. Results and Discussion

An excitonic diffraction grating is a periodic set of stripes with different excitonic properties. When light falls on such a structure with a resonant wavelength, excitons are excited. The resulting macroscopic polarization leads to the appearance of the secondary electrical field in the form of reflected and transmitted waves, and also additional diffracted plane waves due to the periodical spatial modulation of the exciton ensemble. The diffraction disappears away from the excitonic resonance. To create such a resonant diffraction grating, it is necessary to choose a material with pronounced exciton properties, and spatially modulate these properties by some method. In this work, three-dimensional halide perovskite $CsPbBr_3$ was chosen as such a material, and broadening of exciton resonances due to ion-irradiation-induced defect formation was chosen as a modulation method.

In order to create excitonic DOE single crystals of fully inorganic halide perovskite $CsPbBr_3$ were grown from a solution of salts in HBr (see Experimental Section). The size of the crystals was several mm (Figure S1, Supporting Information). Modulation of excitonic properties was made by the irradiation of the sample with 30 keV Ga^+ ions with the dose 10^{14} cm^{-2}. This dose is two orders of magnitude less than the dose leading to the sample milling.[30,31] Thus, irradiation led only to local implantation and defect formation.

The spatial resolution of the irradiation could be estimated from the Monte Carlo simulation. **Figure 1**b shows the simulated vacancies generation yield in $CsPbBr_3$ crystal irradiated with the 30 keV Ga^+ ions. Around 600 vacancies per implanted ion were generated according to the simulation. In Figure S2, Supporting Information the convolution of the simulated distribution with the step function is shown. It can be seen that the theoretical resolution is sub-wavelength for the visible light.

The patterns irradiated on the sample were 100 × 100 µm areas filled with stripes with $L = 5$ µm period and 2.5 µm width. In Figure 1, a scanning electron microscopy (SEM) image of an irradiated area is shown in the material contrast mode using the in-lens detector. It can be seen that the irradiation leads to the contrast change, with irradiated areas appearing brighter. Such contrast corresponds to heavier and denser elements and could be explained by the removal of absorbed molecules and synthesis residuals. The sample relief did not change.

For optical studies, the sample was kept in a cryostat at temperature $T = 4$ K. Ion irradiation with such doses does not significantly quench the photoluminescence (PL) signal but leads to the appearance of a long-wavelength defect-related tail.[28] Thus, for energies well below the exciton resonance PL signal increases. This effect could be used for the visualization of irradiated areas. Figure 1c–e shows PL maps of the grating (Figure 1f). In Figure 1c a PL map without filtering shows a slight decrease of the PL intensity in the irradiated area. In the case of $E < 2.21$ eV filter (Figure 1d) irradiated and other defect areas looks brighter. Finally for $E < 2.14$ eV filter (Figure 1e) the irradiated grating is the most bright object. Grating stripes are visible in filtered PL maps.

To determine the spectral position of the exciton resonance, the reflection spectrum from the sample was measured. **Figure 2**b shows the normal reflection spectrum $K_R = \frac{I_R}{I_0}$ from the non-irradiated part of the sample, where I_0 and I_R are incident and reflected intensities correspondingly. The main observable feature, that is, the state with the highest oscil-

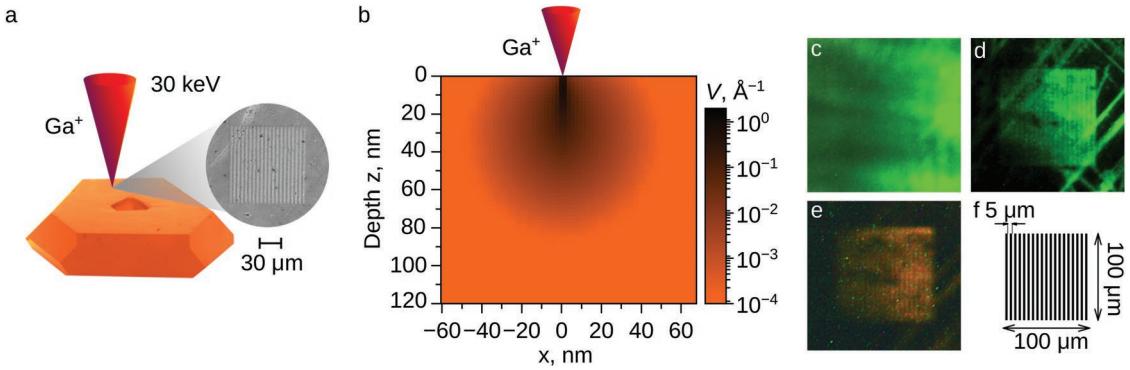

Figure 1. a) Ion beam irradiation of the $CsPbBr_3$ sample (colorized SEM image). The magnified area shows the SEM image of the irradiated grating. b) Vacancies generation yield V for the 30 keV Ga^+ irradiation of $CsPbBr_3$. c–e) PL maps of the grating without filter (c) and with $E < 2.21$ eV (d) and $E < 2.14$ eV (e) filters. f) Irradiation scheme of the grating, black areas were irradiated.

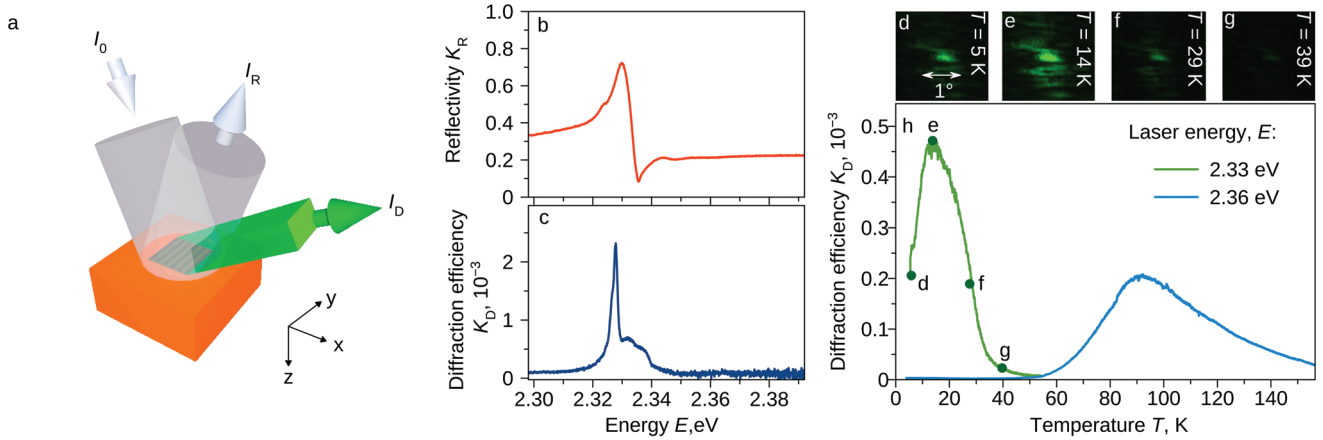

Figure 2. a) Optical experiment scheme: a full spectrum of light is reflected from the sample close to normal geometry and only a spectrally narrow part is diffracted from the grating (angles are shown not to scale). I_0, I_R, and I_D are incident, reflection, and diffraction intensities. b) Reflectivity and c) diffraction efficiency spectra for $T = 4$ K. d–g) Angular distribution of $k = 9$ diffraction reflex at different temperatures for the normal incident light with $E = 2.33$ eV. h) Temperature dependency of the diffraction efficiency for incident light with $E = 2.33$ eV (green) and $E = 2.36$ eV (blue). Dots denote temperatures corresponding to angular distributions (d)–(g).

lator strength, is the free exciton resonance[13,16] with energy $E_{exc} \approx 2.3$ eV. The ion irradiation leads to the periodic spatial modulation of excitonic properties. Illumination of the modulated area with light close to the exciton resonance ($E \approx E_{exc}$) results in the formation of new coherent response—a diffraction reflex (Figure 2a). The unique feature of this response is the absence of non-resonant diffraction due to the absence of the sample relief modulation.

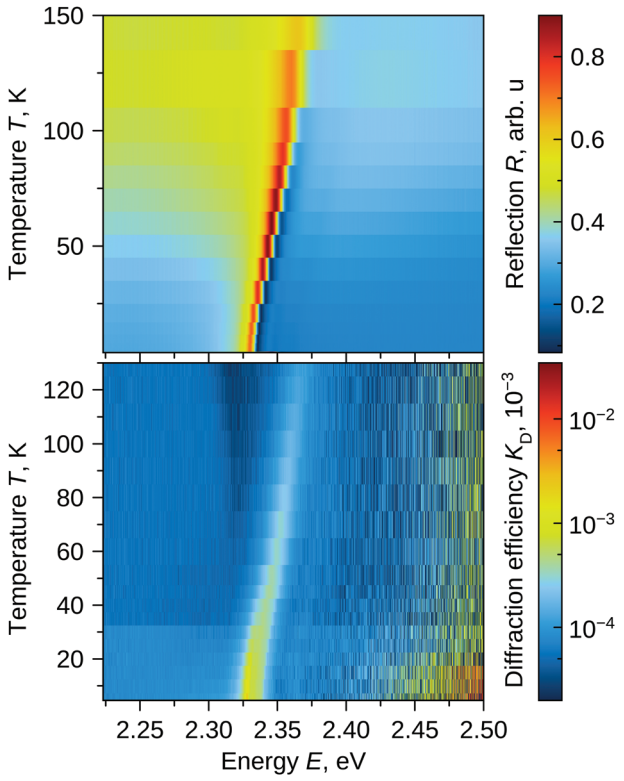

Figure 3. Temperature dependencies of a) reflectivity K_R and b) diffraction efficiency K_D spectra.

For normal incidence, the diffraction angle for the kth diffraction maximum will be $\alpha = \arcsin\left(\frac{k\lambda_{exc}}{L}\right)$, where λ_{exc} is the exciton resonance wavelength. Cryostat geometry makes it possible to observe the $k = 9$ diffraction reflex with $\alpha = 77°$. To find the diffraction reflex, the grating was illuminated by a plane wavefront of cw-laser with energy $E = 2.33$ eV along the normal direction. Since this energy is close to the exciton energy, we were able to observe a distinct diffraction reflex. The angular width of the reflex was ≈1° (Figure 2d–g).

A more precise adjustment of the excitation to the exciton resonance can be done by tuning the latter by varying the sample temperature. Figure 2h shows the temperature dependency of the diffraction efficiency $K_D = \frac{I_D}{I_0}$, where I_D is the diffracted light intensity. The diffraction efficiency reaches its maximum at $T = 14$ K, and the angular distribution of diffraction does not depend on temperature (Figure 2d–g). The same behavior was observed for a laser with a higher energy $E = 2.36$ eV with maximum diffraction efficiency at higher temperature $T = 92$ K. The higher resonant temperature for a higher energy laser is due to the fact that in halide perovskites the band gap increases with temperature. This also could be seen in the temperature dependence of the reflection spectrum $K_R(T)$ in **Figure 3**a.

Identification of the direction of the diffraction reflex made it possible to measure the full diffraction spectrum $K_D(E)$. In Figure 2c the diffraction spectrum is shown for $T = 4$ K. The free exciton resonance dominates this spectrum. The level of background non-resonant signal is less than 10^{-4} and is associated with scattering on a non-ideal sample surface since it is observed not only in the direction of diffraction. Thus, the observed spectrum fully corresponds to the concept of resonant diffraction. Temperature dependency of diffraction spectrum (Figure 3b) shows that resonant diffraction is quite distinguishable at temperatures of 120 K and even above (see blue curve in Figure 2h). Several weaker resonant features are observed in diffraction spectra at energies above the exciton resonance.

The fitting allows us to isolate these features (Figure S4a, Supporting Information). The study of these states is beyond the scope of this work, but they are presumably related to the excited states of the exciton with temperature-independent splittings of 5 meV scale (Figure S4d, Supporting Information).

3. Conclusion

In this work, we have demonstrated an exciton diffraction grating based on a single crystal of a fully inorganic halide perovskite $CsPbBr_3$. Such grating is an example of the simplest resonant DOE. For spatial modulation of exciton properties without changing the relief of the sample, we used irradiation with a focused 30 keV Ga^+ ion beam with a dose two orders of magnitude lower than the milling dose. The simulation shows that such a method could be used to create defective regions with a subwavelength spatial resolution. A grating with 5 μm period made it possible to observe a narrow and directed diffraction reflex due to the spatial modulation of the properties of free excitons and higher energy states. The total spectral width of free excitons diffraction was 1.7 meV, and the maximum diffraction efficiency reached 2.3×10^{-3}. Halide perovskite exciton DOEs will make it possible to create active elements for information photonics with simple synthesis, efficient interaction with light, and nonlinear properties.

4. Experimental Section

Synthesis and Characterization: $CsPbBr_3$ halide perovskite single crystals were grown from a solution using concentrated acid: 0.6 g (2.8 mmol) of CsBr and 1.03 g (2.8 mmol) of $PbBr_2$ were dissolved in 10 mL of concentrated hydrobromic acid HBr. The solution was left at room temperature for 16 h until single crystals were obtained. The resulting crystals were filtered, washed with ethanol, and stored in a dry atmosphere. The formation of the single $CsPbBr_3$ perovskite phase was confirmed by X-ray diffraction (Figure S5, Supporting Information).

Ion Beam Irradiation: $CsPbBr_3$ single crystals were irradiated by 30 keV Ga^+ ions at room temperature in the Zeiss Crossbeam 1540XB workstation combining a scanning electron microscope and a FIB column. For controlled exposure, an external scan generator Raith ELPHY Plus and an electrostatic beam blanker were used. The irradiated pattern was an array of 20 stripes with 2.5×100 μm size and 2.5 μm gaps between stripes (Figure 1f). Thus, diffraction gratings with a period of 5 μm (200 mm^{-1}) and 100×100 μm size were fabricated. Stripes were irradiated by ion dose 10^{14} cm^{-2}. The ion beam was focused in the 20 nm spot. The 200 pA ion beam current was used. The same workstation was used for SEM images captured in the material contrast mode (InLens detector).

Ion-Sample Interaction Modeling: To simulate ion scattering and defect formation, the Monte Carlo method implemented in the SRIM 2013 program[33] was used. Modeling by this method does not take into account the crystal structure of the material and ion channeling. A beam of 30 keV Ga^+ ions (68.93 amu) hitting the 200 nm-thick $CsPbBr_3$ target normal to the surface, was modeled. The density of the material was taken to be 4.856 g cm^{-3}.[34] The target consisted of 20% Cs (132.91 amu), 20% Pb (207.19 amu), and 60% Br (79.904 amu). For all elements, the lattice binding energy was set to 3 eV and the displacement energy was 25 eV. Detailed calculations with full damage cascades were performed for 10^6 incident ions. Sputtering effects were not considered. Based on the simulations, the vacancy generation yields $V(z)$ (vacancies/(Å· ion)) for Cs, Pb, and Br atoms at a given target depth z were obtained. Multiplying this value by the layer thickness and the irradiation dose provides the vacancy density in the layer at the given depth. Nuclear energy loss predicted by the method used in [reference srim above] is 780 eV nm^{-1}. The corresponding projected range of Ga^+ ions is 24 nm.

*Optical Study:*For optical research, the crystal was mounted in a Montana Instruments closed-cycle helium cryostat and cooled down to $T = 4$ K. PL mapping was carried out by the illumination of the sample by a 450 nm cw-laser and collecting PL by a color CMOS camera with different long pass filters. To measure the reflectivity and diffraction efficiency spectra, a green LED was used as a source. Using a telescope with a diaphragm at the focus, a parallel beam was made that fell on the sample. A spectrometer with a CCD detector was used to capture spectra. To visualize the diffraction reflex, 532 and 525 nm lasers were used.

Supporting Information

Supporting Information is available from the Wiley Online Library or from the author.

Acknowledgements

This research has been supported by the Ministry of Science and Higher Education of the Russian Federation (Megagrant no. 075-15-2022-1112). This work was carried out on the equipment of the SPbU Resource Centers "Nanophotonics" and "X-Ray Diffraction Studies" and using research facilities of the laboratory "Photoactive Nanocomposite Materials" (SPbU ID: 91696387).

Conflict of Interest

The authors declare no conflict of interest.

Data Availability Statement

The data that support the findings of this study are available in the supplementary material of this article.

Keywords

defects, diffractive optical elements, excitons, focused ion beams, halide perovskites

Received: September 13, 2022
Revised: November 22, 2022
Published online: December 22, 2022

[1] S. V. Poltavtsev, V. V. Ovsyankin, B. V. Stroganov, *Phys. Status Solidi C* **2009**, *6*, 483.
[2] S. V. Poltavtsev, B. V. Stroganov, *Phys. Solid State* **2010**, *52*, 1899.
[3] S. Poltavtsev, Y. Efimov, Y. Dolgikh, S. Eliseev, V. Petrov, V. Ovsyankin, *Solid State Commun.* **2014**, *199*, 47.
[4] Y. V. Kapitonov, M. A. Kozhaev, Y. K. Dolgikh, S. A. Eliseev, Y. P. Efimov, P. G. Ulyanov, V. V. Petrov, V. V. Ovsyankin, *Phys. Status Solidi B* **2013**, *250*, 2180.
[5] Y. V. Kapitonov, P. Y. Shapochkin, Y. V. Petrov, Y. P. Efimov, S. A. Eliseev, Y. K. Dolgikh, V. V. Petrov, V. V. Ovsyankin, *Phys. Status Solidi B* **2015**, *252*, 1950.

[6] Y. V. Kapitonov, P. Y. Shapochkin, L. Y. Beliaev, Y. V. Petrov, Y. P. Efimov, S. A. Eliseev, V. A. Lovtcius, V. V. Petrov, V. V. Ovsyankin, *Opt. Lett.* **2016**, *41*, 104.
[7] P. Y. Shapochkin, Y. V. Petrov, S. A. Eliseev, V. A. Lovcjus, Y. P. Efimov, Y. V. Kapitonov, *J. Opt. Soc. Am. A* **2019**, *36*, 1505.
[8] V. G. Davydov, S. A. Gavrilov, G. G. Kozlov, B. V. Stroganov, S. V. Poltavtsev, V. V. Ovsyankin, *Opt. Spectrosc.* **2009**, *107*, 981.
[9] A. K. Jena, A. Kulkarni, T. Miyasaka, *Chem. Rev.* **2019**, *119*, 3036.
[10] L. Chouhan, S. Ghimire, C. Subrahmanyam, T. Miyasaka, V. Biju, *Chem. Soc. Rev.* **2020**, *49*, 2869.
[11] H. Dong, C. Zhang, X. Liu, J. Yao, Y. S. Zhao, *Chem. Soc. Rev.* **2020**, *49*, 951.
[12] I. Shishkin, A. Polushkin, E. Tiguntseva, A. Murzin, B. Stroganov, Y. Kapitonov, S. A. Kulinich, A. Kuchmizhak, S. Makarov, *Appl. Phys. Express* **2019**, *12*, 122001.
[13] A. O. Murzin, B. V. Stroganov, C. Günnemann, S. B. Hammouda, A. V. Shurukhina, M. S. Lozhkin, A. V. Emeline, Y. V. Kapitonov, *Adv. Opt. Mater.* **2020**, *8*, 2000690.
[14] C. Huang, C. Zhang, S. Xiao, Y. Wang, Y. Fan, Y. Liu, N. Zhang, G. Qu, H. Ji, J. Han, L. Ge, Y. Kivshar, Q. Song, *Science* **2020**, *367*, 1018.
[15] W. Sun, Y. Liu, G. Qu, Y. Fan, W. Dai, Y. Wang, Q. Song, J. Han, S. Xiao, *Nat. Commun.* **2020**, *11*, 4862.
[16] J. Tilchin, D. N. Dirin, G. I. Maikov, A. Sashchiuk, M. V. Kovalenko, E. Lifshitz, *ACS Nano* **2016**, *10*, 6363.
[17] O. A. Lozhkina, V. I. Yudin, A. A. Murashkina, V. V. Shilovskikh, V. G. Davydov, R. Kevorkyants, A. V. Emeline, Y. V. Kapitonov, D. W. Bahnemann, *J. Phys. Chem. Lett.* **2018**, *9*, 302.
[18] A. Miyata, M. Anatolie, P. Plochocka, O. Portugall, J. Wang, S. Stranks, H. Snaith, R. J. Nicholas, *Nat. Phys.* **2015**, *11*, 582.
[19] H. Diab, G. Trippé-Allard, F. Lédée, K. Jemli, C. Vilar, G. Bouchez, V. L. Jacques, A. Tejeda, J. Even, J.-S. Lauret, E. Deleporte, D. Garrot, *J. Phys. Chem. Lett.* **2016**, *7*, 5093.
[20] J. Blancon, A. Stier, H. Tsai, W. Nie, C. Stoumpos, B. Traoré, L. Pedesseau, M. Kepenekian, F. Katsutani, G. Noe, J. Kono, S. Tretiak, S. Crooker, C. Katan, M. Kanatzidis, J. Crochet, J. Even, A. Mohite, *Nat. Commun.* **2018**, *9*, 2254.
[21] M. Hirasawa, T. Ishihara, T. Goto, *J. Phys. Soc. Jpn.* **1994**, *63*, 3870.
[22] J. Xu, X. Li, J. Xiong, C. Yuan, S. Semin, T. Rasing, X.-H. Bu, *Adv. Mater.* **2020**, *32*, 1806736.
[23] R. S. Nazarov, I. A. Solovev, A. O. Murzin, N. I. Selivanov, J. Even, A. V. Emeline, Y. V. Kapitonov, *Phys. Rev. B* **2022**, *105*, 245202.
[24] V. V. Belykh, M. L. Skorikov, E. V. Kulebyakina, E. V. Kolobkova, M. S. Kuznetsova, M. M. Glazov, D. R. Yakovlev, *Nano Lett.* **2022**, *22*, 4583.
[25] G. Garcia Arellano, G. Trippé-Allard, T. Campos, F. Bernardot, L. Legrand, D. Garrot, E. Deleporte, C. Testelin, M. Chamarro, *Nanomaterials* **2022**, *12*, 8272.
[26] M. S. Alias, Y. Yang, T. K. Ng, I. Dursun, D. Shi, M. I. Saidaminov, D. Priante, O. M. Bakr, B. S. Ooi, *J. Phys. Chem. Lett.* **2016**, *7*, 137.
[27] M. S. Alias, I. Dursun, D. Shi, M. I. Saidaminov, E. M. Diallo, D. Priante, T. K. Ng, O. M. Bakr, B. S. Ooi, *J. Vac. Sci. Technol., B* **2015**, *33*, 051207.
[28] V. I. Yudin, M. S. Lozhkin, A. V. Shurukhina, A. V. Emeline, Y. V. Kapitonov, *J. Phys. Chem. C* **2019**, *123*, 21130.
[29] O. Plantevin, S. Valàre, D. Guerfa, F. Lédée, G. Trippé-Allard, D. Garrot, E. Deleporte, *Phys. Status Solidi B* **2019**, *256*, 1900199.
[30] Y. Wang, Z. Gu, Y. Ren, Z. Wang, B. Yao, Z. Dong, G. Adamo, H. Zeng, H. Sun, *ACS Appl. Mater. Interfaces* **2019**, *11*, 15756.
[31] M. Palei, M. Motapothula, A. Ray, A. L. Abdelhady, L. Lanzano, M. Prato, J. K. Panda, A. Scarpellini, V. Pellegrini, D. Primetzhofer, U. Petralanda, L. Manna, Z. Dang, *J. Mater. Chem. C* **2020**, *8*, 9923.
[32] J. Kang, L.-W. Wang, *J. Phys. Chem. Lett.* **2017**, *8*, 489.
[33] J. F. Ziegler, M. Ziegler, J. Biersack, *Nucl. Instrum. Methods Phys. Res., Sect. B* **2010**, *268*, 1818.
[34] Y. Rakita, S. R. Cohen, N. K. Kedem, G. Hodes, D. Cahen, *MRS Commun.* **2015**, *5*, 623.